Design analysis and experimental verification of vibration reduction of spatial composite damping truss structure

Haitao Luo[1] [iD]**, Jia Fu[1]** [iD]**, Peng Wang[2] and Haonan Wang[2]**

Abstract

In order to solve the problem that the photoelectric instrument may fail when the vibration response of the truss composite structure is too large, the method of applying the viscoelastic-constrained damping layer on the truss wall and the box panel is used to reduce the vibration of the whole structure. In this article, a broken long tube with viscoelastic-constrained damping layer is introduced. The long tube of the original structure is broken into two identical short tubes, and a tube with free damping layer is added to the junction of the two short pipes, which is connected by adhesive and broken long pipe. By analyzing the frequency response of the traditional space truss and spaceflight load structure, and a broken long tube structure, the acceleration response cloud diagram and the acceleration response curve of the fixed measuring node are obtained. Experiments were carried out to verify the feasibility of the structure. The test results show that the method of broken long pipe with viscoelastic-constrained damping layer can achieve better damping effect than the traditional truss structure, and it can effectively reduce the vibration level of the space load at the end of the truss, and has important reference significant for the vibration reduction design of other space structures.

Introduction

With the development of spacecraft toward the direction of large scale and complexity, the space truss has been applied more and more widely because of its easy disassembly, good technology, light weight, and the ability to adjust the structure according to the specific needs. It is also an important part of the International Space Station as shown in Figure 1. The space truss is mainly used in two aspects. One is to connect the related optoelectronic equipment at the top of the space truss to separate the electronic equipment so as to reduce the interference between each other. The other is as a supporting structure to support large deployable antennas in space and solar panels on satellites.

The space truss and its load are launched through the launch vehicle. The vibration environment experienced by the launch vehicle is mainly divided into random vibration environment and low-frequency sinusoidal vibration environment.[1] Random vibration

[1]State Key Laboratory of Robotics, Shenyang Institute of Automation, Chinese Academy of Sciences (CAS), Shenyang, China
[2]School of Mechanical Engineering and Automation, Northeastern University, Shenyang, China

Corresponding author:
Jia Fu, State Key Laboratory of Robotics, Shenyang Institute of Automation, Chinese Academy of Sciences (CAS), Shenyang 110016, China.
Email: fujia@sia.cn

Figure 1. Space station truss structure.

is mainly caused by engine exhaust noise during take--off, aerodynamic noise in transonic flight section, and pressure pulsation in the combustion chamber of the engine. The low-frequency sinusoidal vibration is mainly caused by the pogo vibration, engine start, flameout, and interstage separation of the projectile structure; the low-order modal free oscillation is caused by the gust and the shock wave oscillation in the transonic flight segment; and low-order longitudinal oscillation is caused by incomplete combustion of the engine. This kind of low-frequency vibration environment will cause the space truss structure to be damaged, the connection will be loose, the structural parts will be deformed, and the performance will be decreased. At the same time, this vibration will cause the precision of the photoelectric instruments to be reduced, mechanical fatigue, short circuit, and open circuit instantly, as well as functional failure.[2] Therefore, it is necessary to study the vibration characteristics and vibration suppression of space truss and its load.[3] There are many literatures on the vibration reduction of space truss structures, which are mainly divided into two categories: damper and damping layer. In previous works,[4–6] dampers were designed according to the structure of the space truss, and the relationship between the placement position of the damper and the damping control effect was studied. YM Park et al.[7] proposed a semi-active control method using dry friction dampers to reduce the transient vibration of the space truss structure. J Yang et al. studied the vibration and damping properties of a hybrid carbon fiber composite pyramidal truss sandwich panel embedded in a viscoelastic layer in a panel. The damping effect of the damping layer is analyzed by simulation and experiment.[8] Based on the modal strain energy (MSE) method, C Liu analyzed the vibration fundamental frequency, loss factor, and resonance response peak of the composite truss structure with different damping layers. The influence of structural parameters and material parameters of damping layer on the damping effect of composite truss was studied.[9] In
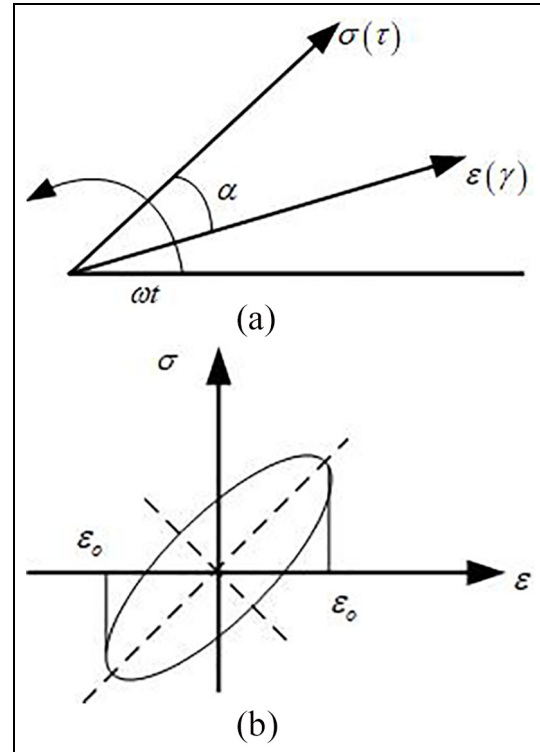
Figure 2. Stress–strain relationship of viscoelastic materials: (a) strain lags behind stress and (b) stress–strain curve.

the traditional space truss, the damping layer is directly applied to the long pipe,[10] and the damping effect is not good due to the long pipe and the large stiffness. In this article, the traditional truss structure is improved, with a free damping layer on the connection of multi-section short pipe, and the growth tube is connected by adhesive and short pipe. The viscoelastic damping layer is applied to the space truss and space load structure for vibration reduction according to actual needs. Through simulation and experimental comparison, the new composite structure is lighter in weight, less rigid, and better in damping effect. Such a complete system of mutual verification of simulation tests has a positive guiding significance for the application of viscoelastic damping layer in aerospace field.

Basic theory of viscoelastic damping materials

When elastic material is subjected to external force,[11] the stress and strain increase or decrease at the same time, the phase of the two is basically the same, and the stress–strain relationship is a straight line. The viscoelastic damping material is different from the elastic material,[12] after the external force is applied. The strain lags behind the stress, and the hysteresis phase angle is

α, as shown in Figure 2(a). The stress–strain relation shows a curve,[13] as shown in Figure 2(b).

The figure area surrounded by the elliptic curve in Figure 2(b) shows the vibration energy consumed by the viscoelastic material after the vibration of the structure. When viscoelastic materials are subjected to external loads to produce elastic deformation, the mathematical expression of stress–strain relationship is as follows[14]

$$\sigma = \sigma_0 e^{iwt} \tag{1}$$

$$\varepsilon = \varepsilon_0 e^{i(wt-\alpha)} \tag{2}$$

In this article, the complex mode method is used to describe the properties of viscoelastic damping materials,[15] according to the definition of complex modulus (tensile modulus)

$$E^* = \frac{\sigma}{\varepsilon} = \frac{\sigma_0}{\varepsilon_0} e^{i\alpha} = E(\cos\alpha + i\sin\alpha) \tag{3}$$

$$E^* = iE'' + E' = E'(1 + i\eta) \tag{4}$$

η is the damping factor of viscoelastic damping material, which can measure the energy consumption ability of viscoelastic damping material.[16] $\eta = E''/E'$, E^* is the complex tensile modulus of viscoelastic damping material; E' is the real part of the complex tensile modulus of viscoelastic damping materials, and E'' is the imaginary part of the complex tensile modulus of viscoelastic damping materials, which determines the energy consumption of viscoelastic damping materials.

If the viscoelastic damping material is subjected to shear deformation, the mathematical expression of the shear stress–strain relationship is as follows[17]

$$\tau = \tau_0 e^{i\omega t} \tag{5}$$

$$\gamma = \gamma_0 e^{i(\omega t-\alpha)} \tag{6}$$

The complex shear modulus is

$$G^* = \frac{\tau}{\gamma} = \frac{\tau_0}{\gamma_0} e^{i\alpha} = G(\cos\alpha + i\sin\alpha) \tag{7}$$

$$G^* = iG'' + G' = G'(1 + i\eta), \eta = G''/G' \tag{8}$$

Among them, G^* is the complex shear modulus of viscoelastic damping material, G' is the real part of the complex shear modulus of viscoelastic damping materials, and G'' is the imaginary part of the complex shear modulus of viscoelastic damping materials, which determines the energy consumption during the conversion of viscoelastic damping materials to thermal energy.

In the practical application of viscoelastic damping materials, it is necessary to decide when to adopt shear modulus, when to adopt tensile modulus, and when to use the relation between shear modulus and tensile modulus according to the specific stress condition.[18]

The mathematical expression of the relationship between shear modulus and tensile modulus is as follows

$$E = 2G(1 + \mu) \tag{9}$$

Among them, μ is Poisson's ratio, general metal material's Poisson's ratio is 0.25:0.35, and viscoelastic damping material's Poisson's ratio is 0.45:0.5.

The energy consumption of viscoelastic damping materials per unit volume during a vibration period under the action of alternating stress and strain can be expressed in terms of ΔW[19]

$$\Delta W = \iint \tau d\gamma dv = \pi\tau_0\gamma_0\alpha = \pi\gamma_0^2 G'' \tag{10}$$

$$\Delta W = \pi\varepsilon_0^2 E'' \tag{11}$$

Where the maximum elastic energy, that is, the total strain energy W within a period

$$W = \frac{1}{2}\gamma_0^2 G' \tag{12}$$

$$W = \frac{1}{2}\varepsilon_0^2 E' \tag{13}$$

Therefore, the ratio of energy consumption to storage energy[20] is

$$\frac{\Delta W}{W} = 2\pi\tan\alpha = 2\pi\eta \tag{14}$$

$$\eta = \frac{\Delta W}{2\pi W} \tag{15}$$

Formula (15) shows that the damping factor η of viscoelastic damping materials is the ratio of the energy consumed by each cycle of vibration to the total strain energy. And the energy consumed by each cycle of vibration is damping energy. Therefore, the larger the damping energy, the greater the damping factor of viscoelastic damping material and the stronger the damping capacity.

The magnitude of damping factor represents the level of damping,[21] which reflects the vibration reduction effect of the structure.

1. MSE method

The damping factor can be easily obtained by the MSE method in the finite element software MSC/NASTRAN.[22]

The damping factor of r-order mode can be expressed as

$$\eta_s^{(i)} = \sum_{j=1}^{n} \eta_{vj} \frac{SE_j^i}{SE^i} \tag{16}$$

where $\eta_s^{(i)}$ is the damping factor of i-order mode, $\eta_{\nu j}$ is the damping factor of the j-species viscoelastic material, SE_j^i represents the r-order mode and strain energy of the j-type viscoelastic materials, SE^i is the total strain energy of the mode i, and n denotes the number of viscoelastic materials.

It can be seen from formula (16) that the damping factor is calculated by the ratio of the viscoelastic damping layer to the energy consumption of the whole structure by the MSE method. The disadvantage of the MSE method is that it is not accurate to assume that the properties of viscoelastic materials do not change with frequency, and the frequency variation of viscoelastic damping materials is not taken into account. In order to solve this problem, the modal damping factor can be simply modified according to the following formula (23)

$$\eta^{(r)'} = \eta^{(r)} \sqrt{\frac{G_2(f_r)}{G_{2,ref}}} \qquad (17)$$

where $\eta^{(r)'}$ is the modified r-order modal damping factor, $\eta^{(r)}$ is the r-order modal damping factor obtained by iterative calculation. $G_{2,ref}$ is the ultimate shear modulus of the damping layer for modal calculation and $G_2(f_r)$ is the shear modulus of damping layer when $f = f_r$, among them, f_r is the r-order frequency obtained by $G_2 = G_{2,ref}$.

2. Complex eigenvalue method (CEM)

Using the complex modulus model, the constitutive relations of viscoelastic materials are as follows[23]

$$\begin{aligned} \sigma_0 &= E^*(\omega)\varepsilon_0 \\ &= [E'(\omega) + iE''(\omega)]\varepsilon_0 \qquad (18) \\ &= E'(\omega)[1 + i\eta(\omega)]\varepsilon_0 \end{aligned}$$

$$\eta(\omega) = \frac{E''(\omega)}{E'(\omega)} \qquad (19)$$

where σ_0 and ε_0 denote the simple harmonic stress and strain with time, $E^*(\omega)$ is the complex modulus of viscoelastic damping material, $E'(\omega)$ and $E''(\omega)$ are real and imaginary parts of complex modulus, and $\eta(\omega)$ is the damping factor of viscoelastic material.

The free vibration equation of viscoelastic damping composite structure is as follows:

$$M\ddot{u}^* + K^*u^* = 0 \qquad (20)$$

$$K^* = K + iK' \qquad (21)$$

where M is the mass matrix, K^* is the complex stiffness matrix, K and K' are the real and imaginary parts of the complex stiffness matrix, and u^* is the node displacement vector.

When $u^* = \phi^* e^{iw^*}t$, the formula (20) may be changed to

$$K^*\phi^* = \lambda^* M\phi^* \qquad (22)$$

Where ϕ^* is the complex eigenvector, $\lambda^* = \omega^{*2}$ is the complex eigenvalue, and ω^* is the complex frequency, the formula (22) is solved by QR matrix decomposition

$$\lambda^* = \lambda + i\lambda' \qquad (23)$$

Thus, the n-order modal damping factor η_n is

$$\eta_n = \frac{\lambda_n'}{\lambda_n} \qquad (24)$$

where λ_n and λ_n' are real and imaginary parts of complex eigenvalues λ_n^*.

The advantage of CEM is that it can describe the dynamic mechanical properties of viscoelastic damping materials.[24] The drawback is that it is necessary to calculate in the complex domain. The eigenvalue and eigenvector are usually complex, which results in a very large amount of computation, which is 5~10 times of the undamped characteristic solution.

The frequency and damping of viscoelastic damping composite structures are calculated by using COMPLEX EIGENVALUE (SOL 107) module in NASTRAN.[25] The concrete method is to establish the finite element model of viscoelastic damping composite structure, and then input the material damping and related material properties of viscoelastic material. In this article, the damping factor is calculated by the CEM. The uncoated viscoelastic damping layer structure is assumed to be undamped structure, and the damping factor is calculated to be an increment of the damping factor.

Design of truss and load structure

For space truss structure modeling and space load, as shown in Figures 3 and 4, the whole structure is made up of long tube, before and after the short tube, cover up and down, left and right sides cover plate, plate, connecting block many parts, fixtures and fittings, standard screw, weighs 15.848 kg, and the material for AL7075.

The structure of the space load box is made of a plate-like structure, with a hollow structure inside, and a screw is used to connect the various surfaces. In addition to the eight faces of the structure of the box structure, the center of the other surfaces has a circular groove with a diameter of 18 mm and a depth of 2 mm. It is used for connecting pieces, connecting the long pipe, short pipe, and connecting block through the connecting piece.
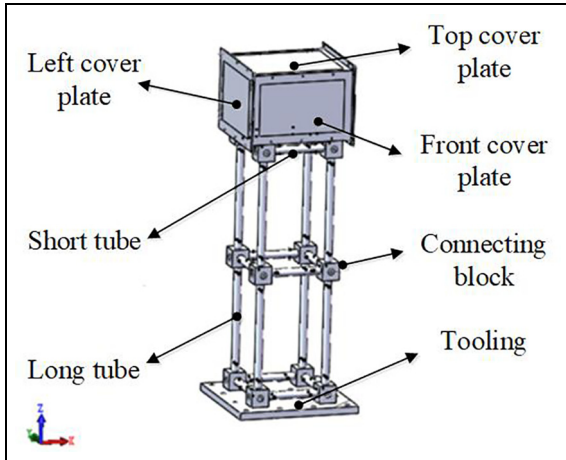
Figure 3. Three-dimensional model.

Figure 4. The connection of connecting block.

The establishment of finite element model

The finite element model adopts the right-hand coordinate system: the origin o is located at the center line of the lower cover plate along the space load length direction, the left cover plate points to the right cover plate and the y axis along the space load width direction, and the front cover plate points to the back cover plate in the positive direction of z axis.

By choosing the international system of units, the mesh is divided by the whole automatic part manually, the mesh elements are triangular and quadrilateral elements, and the connecting blocks and connectors are partitioned by volume mesh, as shown in Figure 5.

The other parts are divided into shell meshes, and the finite element model is shown in Figure 6. The number of units is 338,564, the number of nodes is 162,717, and the weight of the model is 15.23 kg.

A broken long tube structure is introduced. As shown in Figure 7, the long tube of the original structure is broken into two identical short tubes, and a AL7075 tube with a length of 50 mm, an outer diameter of 12 mm, and a wall thickness of 2 mm is added at the junction of the two short tubes. A free damping layer with thickness of 2.5 mm is applied to it, which is connected by adhesive and broken long pipe.

Because the space load box structure is axisymmetric structure, in order to facilitate the study, the upper cover plate, the middle position of the left cover plate and the front cover plate, and the middle position of each long pipe are added with the constrained damping layer in the upper cover plate of the space load box structure, the middle position of the left cover plate, and the front cover plate.

The damping layer uses a volumetric grid, and the constraint layer uses a shell grid with a bias. The elements share nodes, as shown in Figure 8.
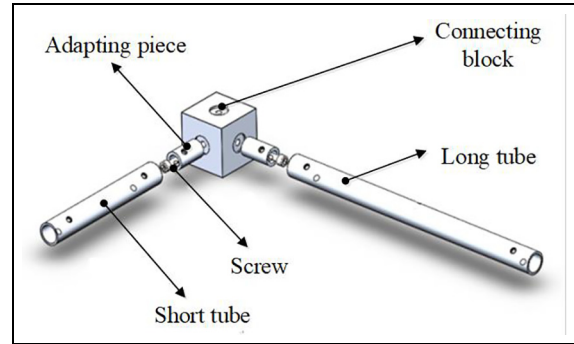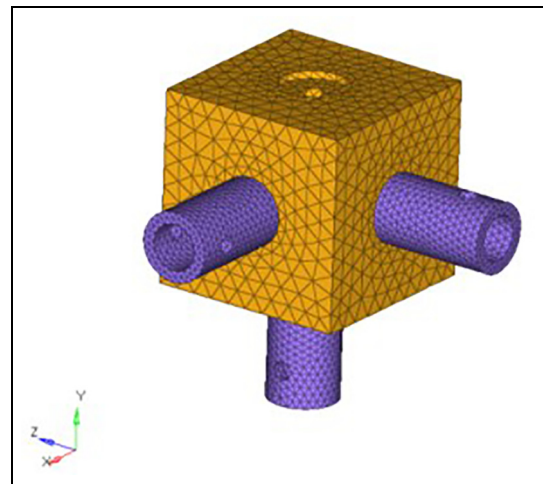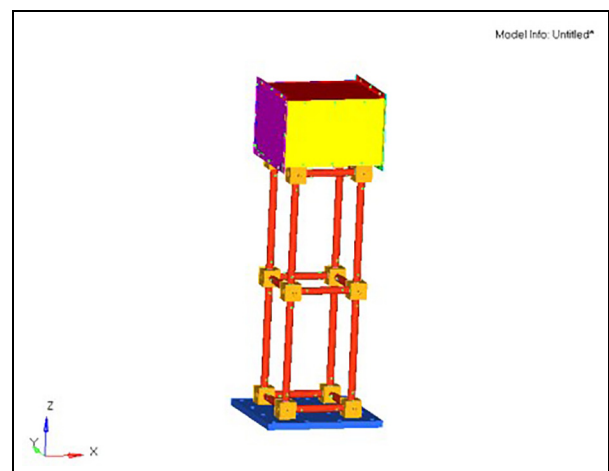

Figure 5. Connection box and connector.

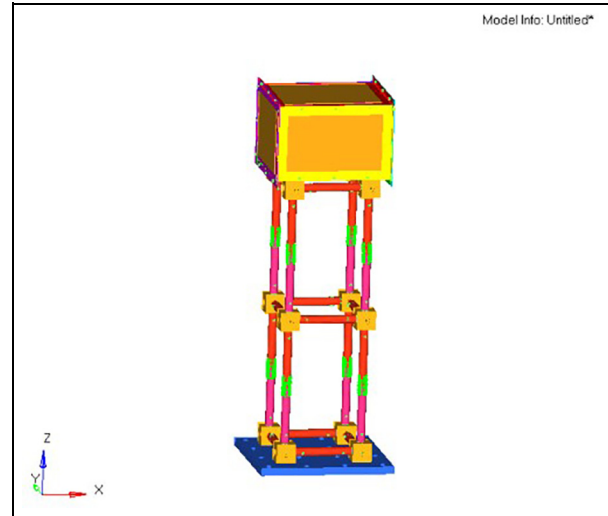Figure 6. Finite element model of the original space truss and aerospace load structure.

The new finite element model of breaking long tube is shown in Figure 9. The number of units is 386,743,

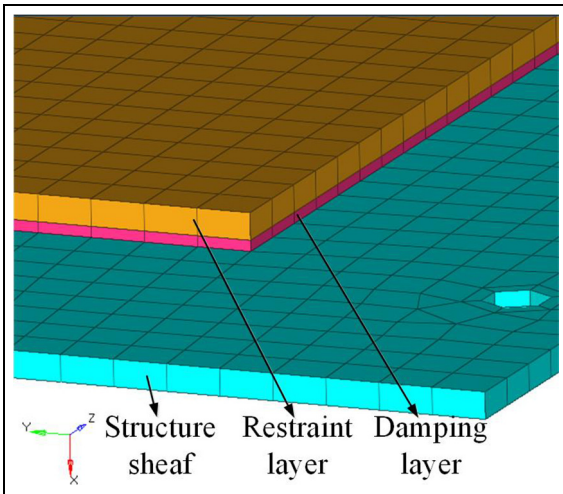**Table 1.** Material properties of damping layer and constrained layer.

Materials (type)	Shear modulus G (MPa)	Modulus of elasticity E (MPa)	Poisson's ratio v	Density ρ (t/mm^3)	Damping factor η
Damping layer (butyl rubber)	1.5	–	0.45	10×10^{-9}	1.05
Restraint layer (Aluminum alloy 7075)	–	7.2×10^4	0.33	2.8×10^{-9}	–
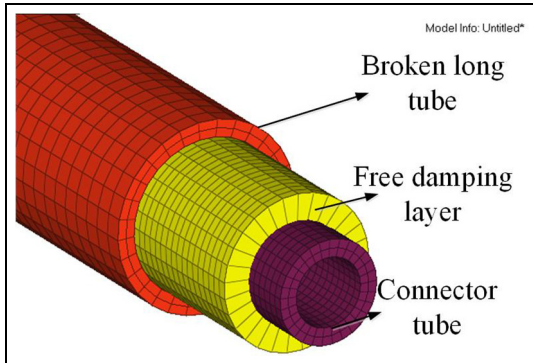
Figure 7. New structure of long tube broken.

Figure 8. Constrained damping layer.

Figure 9. The finite element model of the new structure of break long tube.
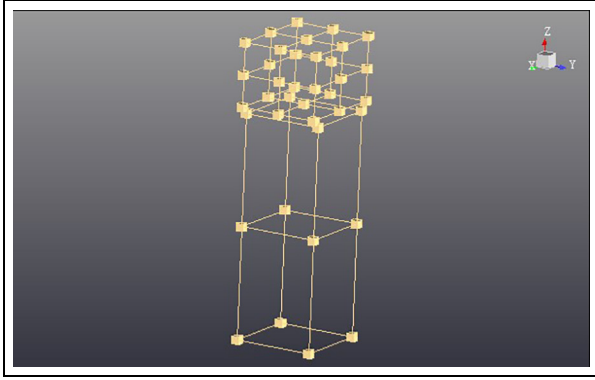

Figure 10. Modal test.

the number of nodes is 193,026, and the new structural model is 16.20 kg.

The damping layer is made from Beijing Institute of Aerospace Materials (703). The thickness of damping layer is 0.8 mm, the material is rubber, and the restraint layer is AL7075 plate with thickness of 2 mm. The material properties of the damping layer and the restraint layer are shown in Table 1.

The modal test

The modal test of truss and load structure is carried out, and the truss structure is fixed to the vibration table. The constraint boundary of the simulated truss structure is shown in Figure 10. The test node layout is shown in Figure 11, with a total of 38 measurement nodes, and the excitation method is used to stimulate. The minimum elastic frequency of the clamping device used for support is much higher than the maximum analysis frequency of the specimen structure. Generally speaking, it is easy to realize the constraint boundary of small and medium structures, but it is difficult to realize the constraint boundary of large structures.[26] The quality of the truss structure in this article is 15.85 kg, the

Figure 11. Geometric model.

analysis frequency is 200 Hz, the vibration table is 4500 kg, and the first-order resonant frequency is 2200 Hz, which satisfies the requirements of the truss structure constraint boundary.

The modal test analysis bandwidth of truss structure is 200 Hz, the frequency resolution is 1 Hz, and the steady-state diagram of the frequency response function (FRF) is shown in Figure 12.

Modal correlation analysis

In this article, modal confidence criterion (MAC) in formula (2) is used as quantitative evaluation index

$$MAC_{Test,FE} = \frac{\left[V_{Test}^T \cdot V_{FE}\right]^2}{\left[V_{Test}^T \cdot V_{test}\right] \cdot \left[V_{FE}^T \cdot V_{FE}\right]} \quad (25)$$

In the formula, V_{test} and V_{FE} are the modal vectors of test mode and finite element modal; the elements in $MAC_{Test,FE}$ matrix represent the cosine angle between two modes, reflecting the relative degree of two modes. The MAC value should be between 0 and 1. When the MAC value is greater than 0.8, it can be considered that the vibration mode V_{test} of the test mode is similar to the mode V_{FE} of the finite element calculation mode; when the MAC value is less than 0.2, it can be considered that the vibration mode of the test mode and the mode of finite element calculation are orthogonal.

In this article, LMS Virtual Lab software is used to conduct correlation analysis based on the results of finite element modal analysis of truss and load structure and modal experimental results. As shown in Table 2, the finite element modal is similar to the experimental mode, and the first two order MAC values are all around 0.9, and the finite element model is acceptable.

## Frequency response analysis of space truss and space load structure

According to the sinusoidal frequency sweep mode of the acceptance stage, the sinusoidal response of the space truss and the spaceflight load structure is analyzed in three directions, and the integral acceleration response cloud diagram is obtained. In order to quantitatively determine the magnitude of acceleration response at a certain position on the space load structure, in this article, the nodes of the front cover, the left cover, and the upper cover of the space truss and the space load structure are selected for analysis, and the acceleration response curves of the fixed measuring nodes are generated. The locations and numbers of the test nodes are shown in Figure 13.

In the finite element model, the corresponding number of measuring nodes 1–4 in three-dimensional (3D) model is 19,545; 27,222; 4912; and 254,679.

The last test node 4 is the basic excitation node. The location of these nodes corresponds to the location of the sensor in the subsequent test, and the location of the measured nodes in the finite element model is shown in Figure 14.

The purpose of this analysis is to determine the acceleration response amplification of the existing space truss and space load structure under the condition of the acceptance stage sinusoidal sweep frequency, on the contrary, to compare the acceleration response data with the structure with viscoelastic damping layer.

The sinusoidal response of the space truss and the spaceflight load structure is analyzed in three directions according to the sinusoidal frequency sweep mode of
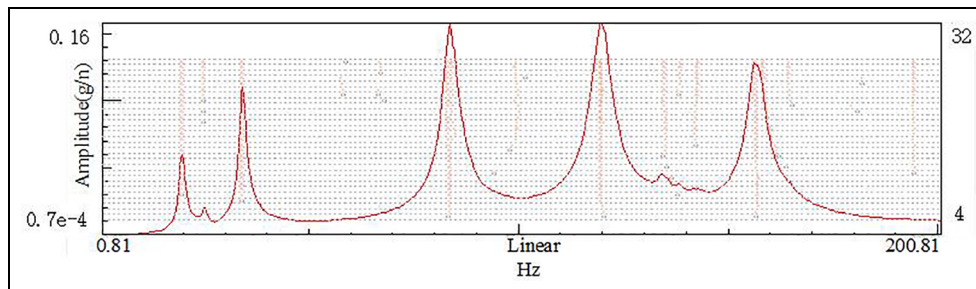
Figure 12. Steady state diagram of frequency response function.

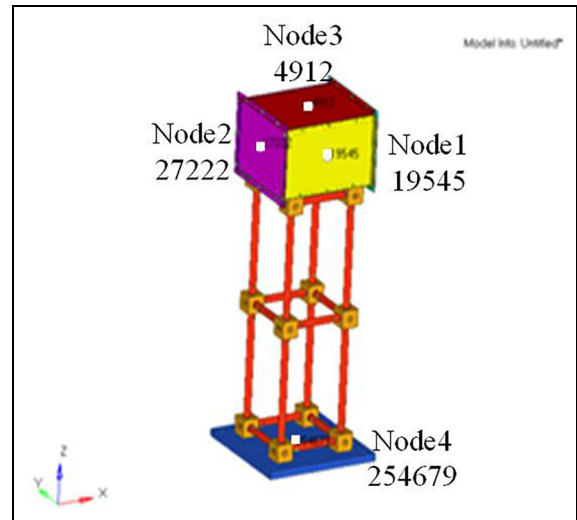**Table 2.** Modal MAC values and frequency differences of modes.

Experimental modal		The simulation mode	Damping ratios	MAC value	Frequency difference (Hz)
Order	Frequency (Hz)	Frequency (Hz)			
1	19.7	25.5	0.55	0.819	−5.75
2	24.9	25.5	0.32	0.924	−0.51
3	34.1	32.3	0.18	0.669	1.83
4	83.6	99.9	0.11	0.519	−16.3
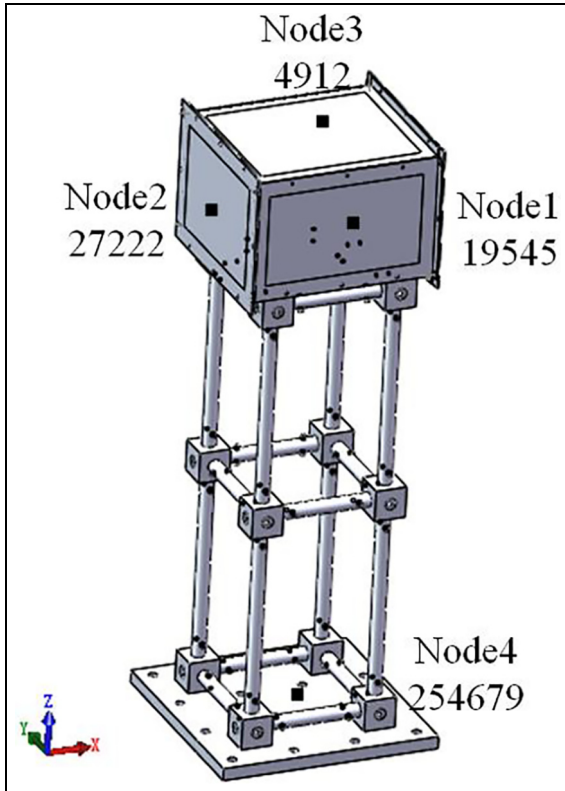
Figure 13. Measuring node position of three-dimensional model.

Figure 14. Measuring node position of finite element model.

Y direction is 17 Hz. The maximum response frequency in Z direction is 99 Hz. The acceleration response of the whole space truss and space load structure is shown in each direction at the corresponding maximum frequency, as shown in Figure 17.

The comparison of acceleration response values at measuring node 1 for the original structure and the broken long tube new structure is shown in Table 4.

Vibration test of space truss

Vibration test is a test to evaluate the vibration resistance of a single component or a whole machine structure in a predetermined transportation and service environment.[27] The main parameters of vibration test are amplitude, velocity, and acceleration. There are two common modes of vibration: one is sinusoidal vibration and the other is random vibration. Sinusoidal vibration test is often used in the laboratory. It is the vibration test of the structure under the action of sinusoidal excitation. The sinusoidal vibration can be divided into sweep vibration and constant frequency vibration. Random vibration test is an experiment of structure under random excitation. Random vibration is a kind

the acceptance stage and the specific test conditions as shown in Table 3. Take node 1 as an example to output the acceleration response curve as shown in Figure 15.

By looking at the acceleration response curves of the measured nodes in the 0–200 Hz range, the maximum response frequency of the original structure in the X direction is 22 Hz. The maximum response frequency in the Y direction is 117 Hz. The acceleration response of the whole space truss and space load structure is shown in the corresponding maximum frequency in each direction as shown in Figure 16.

By looking at the acceleration response curves of the measured nodes in the 0–200 Hz range, the maximum response frequency of the new structure in the X direction is 19 Hz. The maximum response frequency in the Y direction is 17 Hz. The maximum response frequency

Table 3. Sine sweep vibration test conditions (acceptance level).

Loading direction	Loading sweep frequency	Frequency range (Hz)	Amplitude (0-P)
Three axes	4 oct/min	4–10 10–200	5 mm 1 g
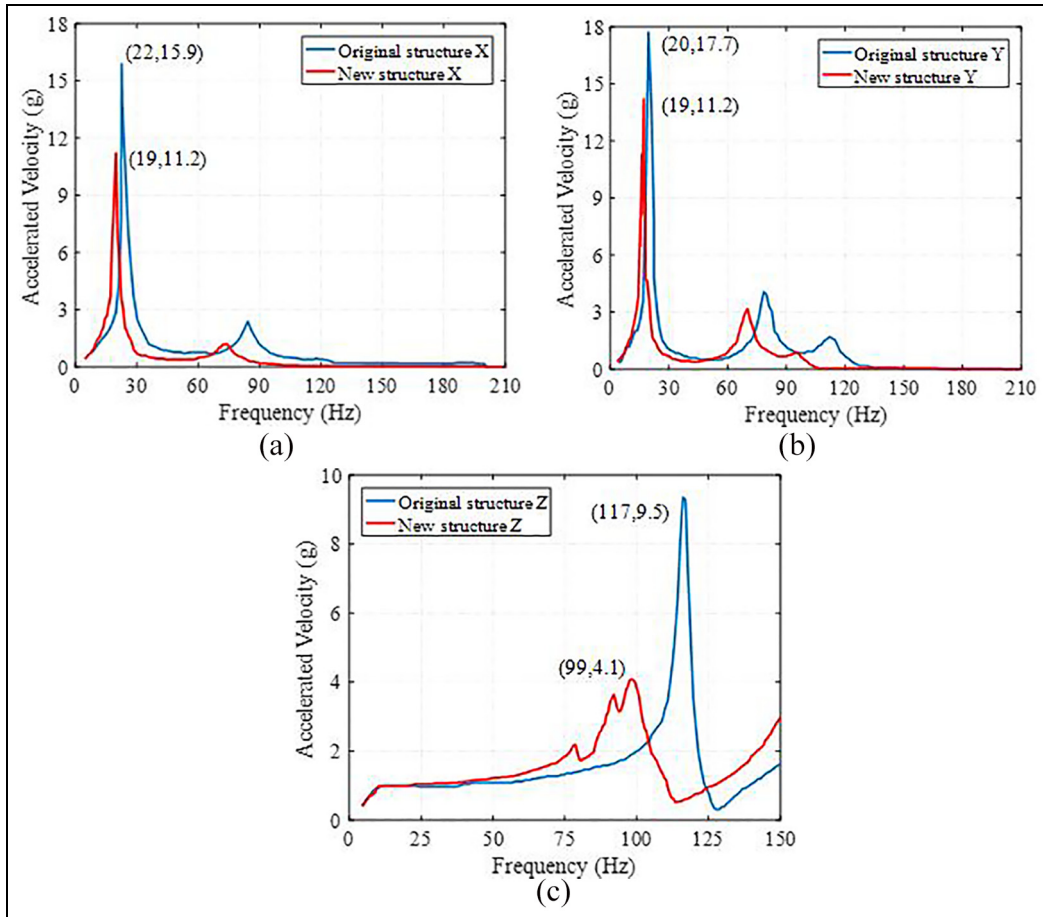
Figure 15. Node 1 acceleration response curve: (a) X direction, (b) Y direction, and (c) Z direction.

of unstable vibration, which can be divided into stationary and non-stationary random vibration.[28]

The experimental objects are the original space truss and spaceflight load structure and the new structure of breaking long pipe, in which the new structure of breaking long tube needs to be coated with constrained damping layer on the space load box structure, as shown in Figures 18 and 19. The free damping layer is added to the connecting pipe. The long pipe is connected by adhesive to the long tube, which is connected by screws to the connecting box through the connector, as shown in Figure 20.

The purpose of the test is to obtain the acceleration response of the original space truss and spaceflight load structure and the new structure with broken long tube in three directions by vibration test. The results are compared with the simulation results. To evaluate the damping effect of the two structures, the photos taken during the experiment are shown in Figure 21.

The test equipment includes electromagnetic shaking table (Space Hill 10t Station, Model H1248a), power amplifier, vibration controller, data acquisition instrument, computer, acceleration sensor, and vibration test equipment as shown in Figure 22.

The specifications, models, and functional parameters of the main instruments used in the whole vibration test process are shown in Table 5 below.

The flow chart for vibration testing and analysis is shown in Figure 23.
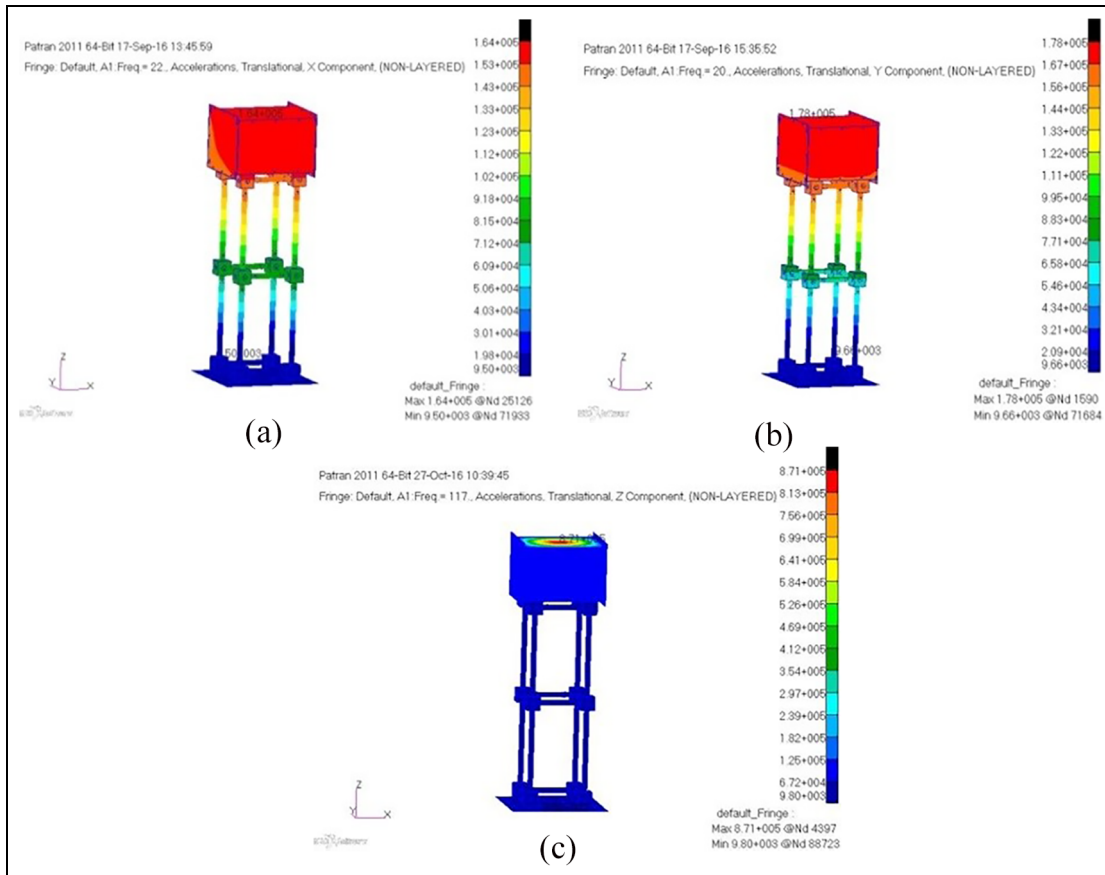
Figure 16. Acceleration response of space truss and space load structure: (a) *X* direction, (b) *Y* direction, and (c) *Z* direction.

FRF analysis mainly obtains the relation between input and output position through the transfer function. FRF is the ratio of the Fourier transform of the response to the Fourier transform of the force or the ratio of the cross-spectrum of the force and response to the self-spectrum of the force. The FRF can be obtained by a dedicated instrument such as an FFT (fast Fourier transform) analyzer or a data acquisition system with FFT function software. The steps to obtain the FRF are as follows. First, an analog signal is obtained from the measuring device. Second, the analog signal is digitally represented by an analog to digital converter. After sampling the data, the FFT is used to obtain the linear amplitude spectrum of the input excitation and the output response. When the power spectrum is calculated from the linear amplitude spectrum, the square of the linear amplitude spectrum is divided by the time length to be the power spectrum. The ratio of the mutual power spectrum of force and response to the self-power spectrum of force is FRF. In the data acquisition and post-processing, four averages are used in the control software to calculate the FRFs in advance. Sufficient average times can improve the precision of data processing and ensure the consistency of curve drawing.

The sinusoidal sweep control signal from the vibration controller is amplified by the power amplifier and transmitted to the vibration table. The electromagnetic vibration table excites the space truss and the space load structure along the *X* direction and *Z* direction, respectively. Some of the acceleration response signals of each measuring channel are transmitted to the vibration controller as feedback signals by the acceleration sensor at the feedback point position to control the vibration table. A part of the acceleration sensor passing through the measuring node position is transferred to the data acquisition instrument, which is amplified and filtered and collected into the computer, and is processed and analyzed on average. The time domain waveforms of acceleration signals and the acceleration frequency response characteristics of the acceleration signals in the 0–200 Hz range relative to the reference channel measurement node 1 are obtained.

The curve of acceleration response of the original space truss and space load structure and the new structure with broken long tube under vibration excitation is shown in Figure 24.

The results of acceleration response of the original design structure of space truss and the new structure of breaking long tube under three directions excitation at
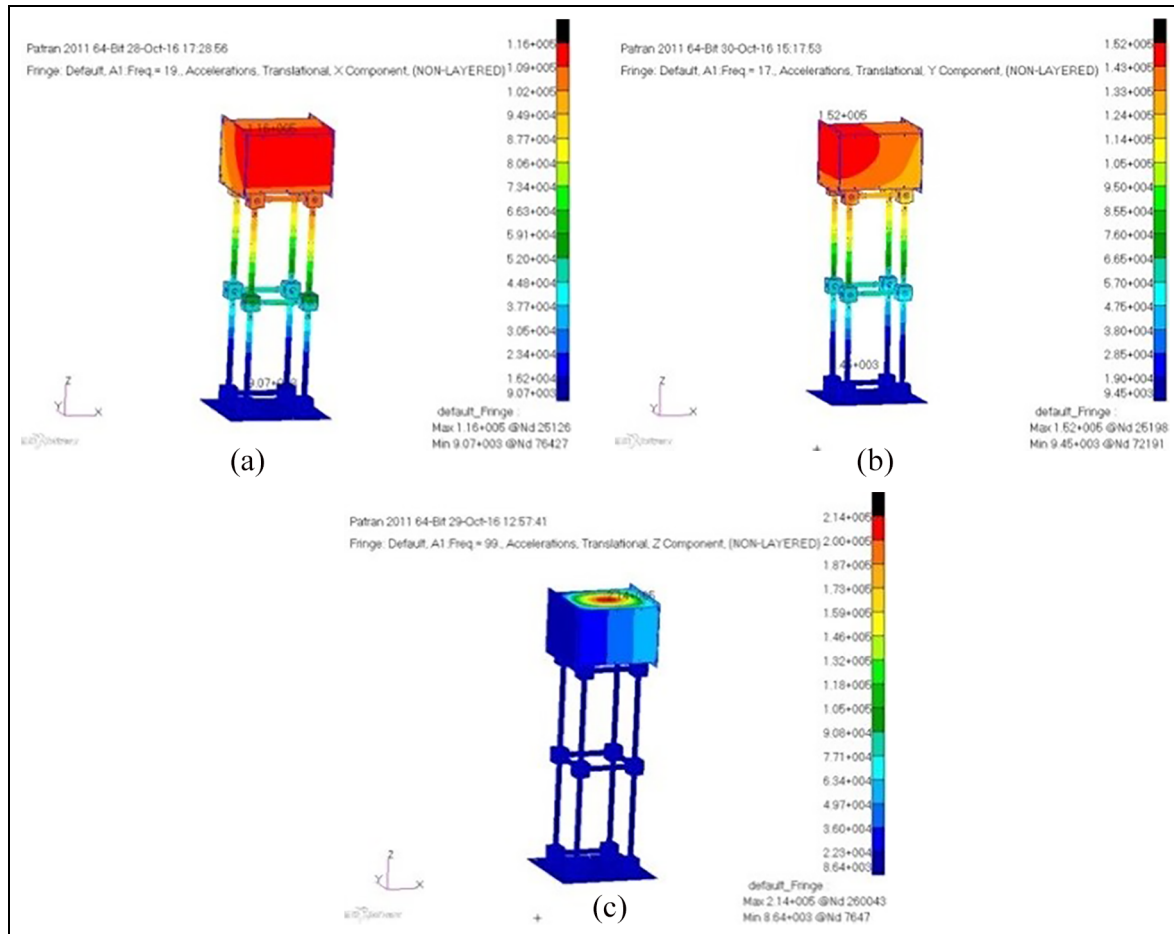
Figure 17. Cloud diagram of acceleration response of a new long tubular structure: (a) *X* direction, (b) *Y* direction, and (c) *Z* direction.

Table 4. Comparison of acceleration response in simulation analysis.

| Excitation direction	Original design structure		New structure		Damping level	
	Frequency (Hz)	Amplitude (g)	Frequency (Hz)	Amplitude (g)	Frequency (Hz)	Amplitude (g)
X	22	15.9	19	11.2	3	4.7
Y	20	17.7	17	14.2	3	3.5
Z	117	9.5	99	4.1	18	5.4

the same measuring node are compared, as shown in Table 6.

By comparing the experimental data of the two design structures, it can be seen that the acceleration response and the maximum acceleration response frequency of the broken long tubular structure in the three directions of 0–200 Hz are lower than those of the original space truss structure. But the resonance frequency is slightly lower. The maximum response frequency of *X* to corresponding acceleration is reduced from 21.61 to 19.15 Hz. The maximum response frequency of *Y* direction acceleration is reduced from 19.69 to 17.09 Hz. The

maximum response frequency of *Z* direction corresponding acceleration is reduced from 128.7 to 110.42 Hz. The damping effect of space truss and space load structure is the most obvious in *Z* direction, and the peak value of acceleration response decreases by more than 56.79%.

Conclusion

In this article, a space truss with long tube broken and its spaceflight load structure are introduced, and the vibration absorption design is carried out by using
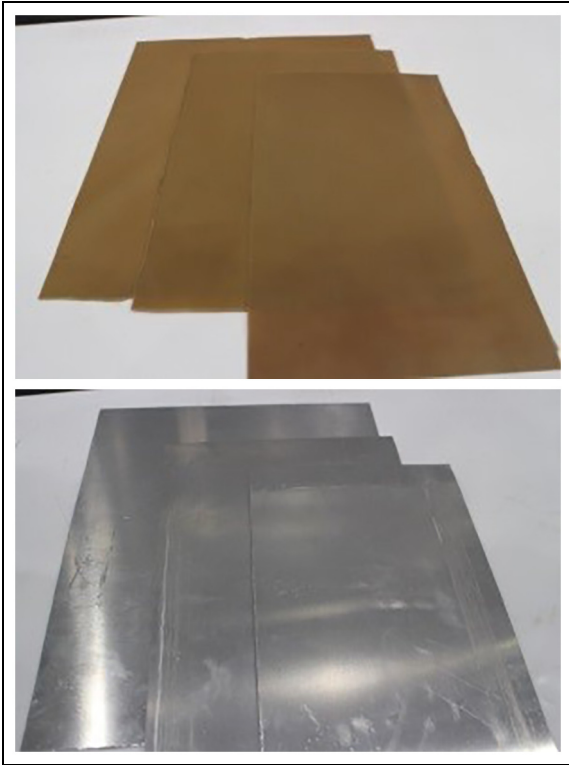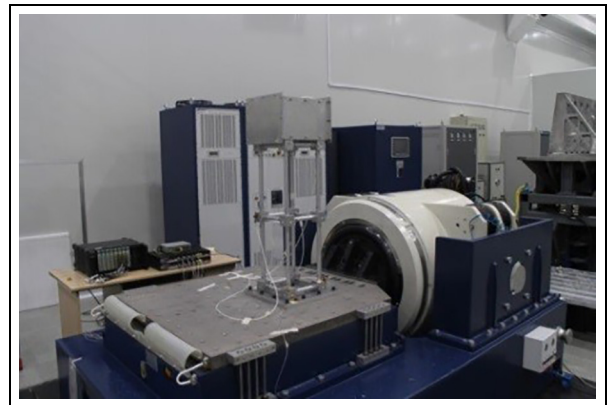
Figure 18. The damping layer and the constrained layer.
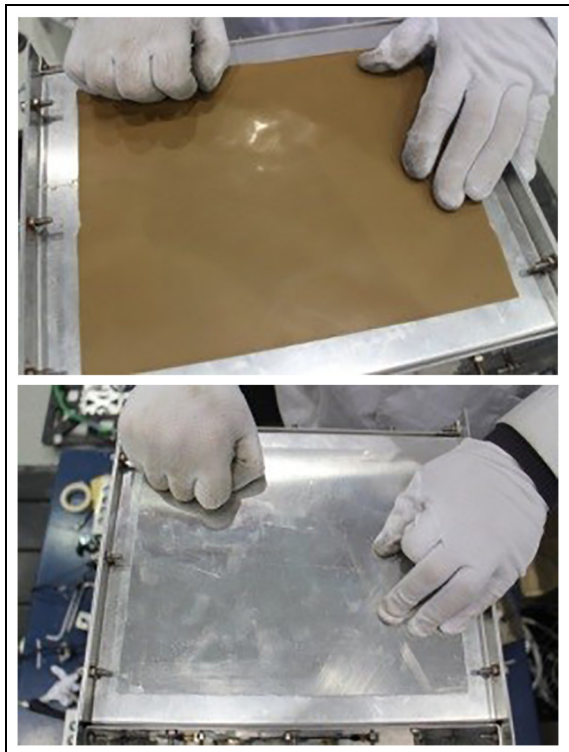
Figure 19. Paste process of damping layer and constrained layer.

Figure 20. The composite structure of long tube damping.


Figure 21. Vibration test field photo.

**Figure 22.** Vibration test equipment.

viscoelastic damping layer. In order to obtain the dynamic characteristics of the structure of the finite element modal analysis and modal test, through determining finite element modal and test modal similar degree is higher, the former two order MAC values are around

Table 5. Specifications, models, and technical parameters of the sensors.

Sensors	Type	Sensitivity	Frequency range
Force	B&K8206	22.5 mm/N	0~10 kHz
Force	B&K8230	110 mm/N	0~75 kHz
Acceleration	B&K4524	10 mmv/G	0.25~3 kHz
Acceleration	B&K4528	10 mmv/G	0.3~10 kHz
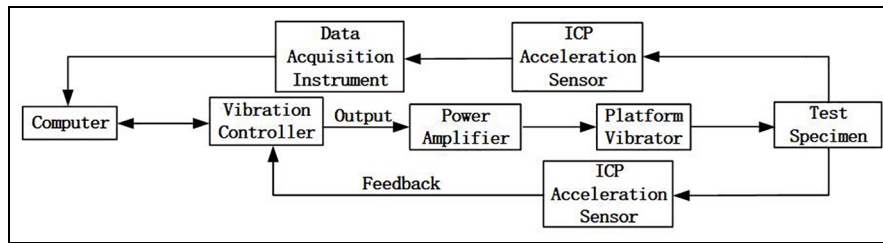
Figure 23. Flow chart of vibration test.
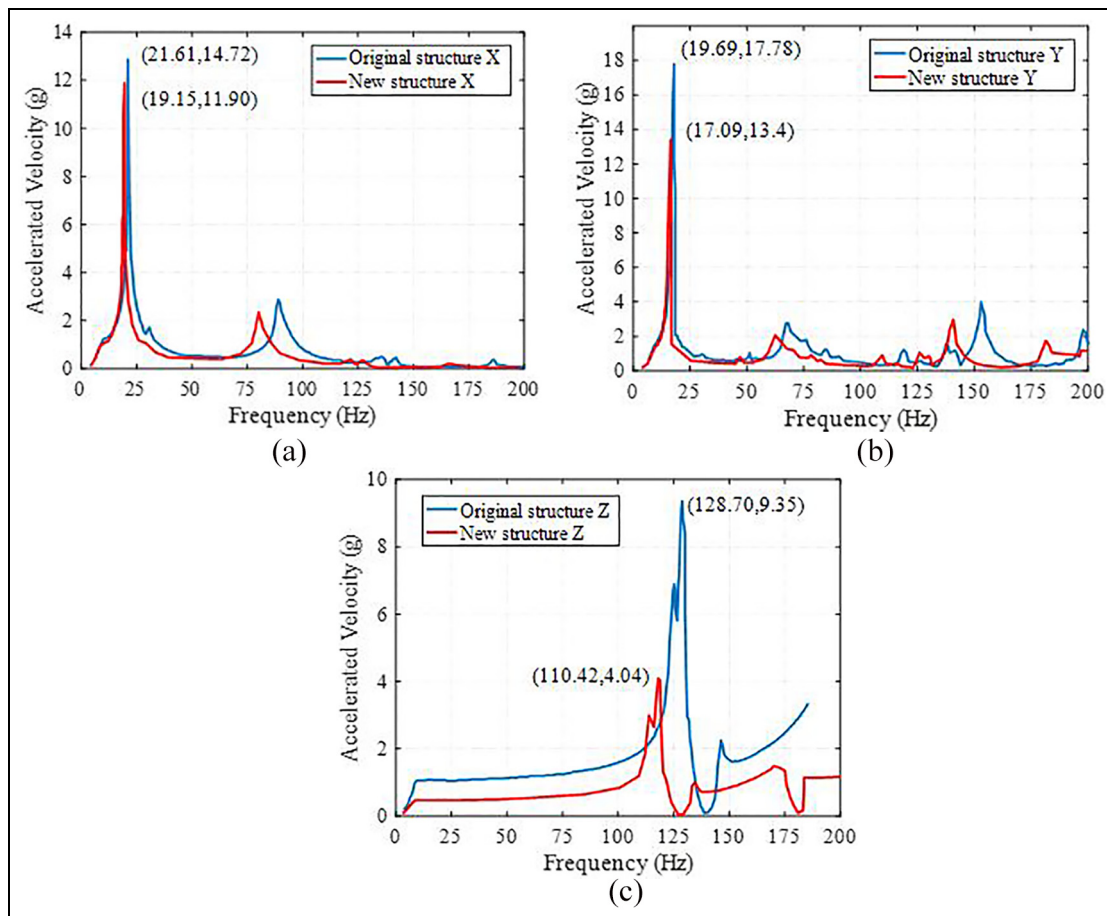
Figure 24. Acceleration response curve of measuring node 1: (a) X direction, (b) Y direction, and (c) Z direction.

0.9; finite element model is acceptable. Then the finite element frequency response analysis of the original model and the new model is carried out, and the acceleration curve at one measuring node and the acceleration response cloud diagram of the two structures are analyzed. The results show that the vibration

Table 6. Comparison of acceleration response in vibration experiment.

Excitation direction	Original design structure		New structure		Damping level	
	Frequency (Hz)	Amplitude (g)	Frequency (Hz)	Amplitude (g)	Frequency (Hz)	Amplitude (g)
X	21.61	14.72	19.15	11.90	2.46	2.82
Y	19.69	17.78	17.09	13.40	2.60	4.38
Z	128.70	9.35	110.42	4.04	18.28	5.31

absorption effect of the new structure with broken long tube is obvious. According to the actual vibration condition, the test results show that the new structure of breaking the long tube and applying the constrained damping layer at the joint has obvious effect on reducing the vibration of the space load. The feasibility of the new structure is verified. In addition, through the analysis of vibration test data, the damping effect of viscoelastic damping layer on space truss and spaceflight load structure is evaluated more intuitively and accurately. It is of great significance for the application of viscoelastic damping materials in space truss structures and similar spacecraft.

Declaration of conflicting interests

The author(s) declared no potential conflicts of interest with respect to the research, authorship, and/or publication of this article.

Funding

The author(s) disclosed the receipt of the following financial support for the research, authorship, and/or publication of this article: This research is supported by the National Natural Science Foundation of China (Grant No.51505470) and Youth Innovation Promotion Association, CAS, and Jiang Xinsong Innovation Fund.

ORCID iDs

Haitao Luo https://orcid.org/0000-0001-8865-6466
Jia Fu https://orcid.org/0000-0003-4216-0064

References

1. Mead DJ and Markus S. The forced vibration of a three-layer, damped sandwich beam with arbitrary boundary conditions. *J Sound Vibrat* 1969; 10: 163–175.
2. Han L, He X, Yang J, et al. Development of a self-moving space manipulator end effector. *Robot* 2016; 38: 720–726.
3. Zhao W. *Vibration analysis and optimization of sandwich structure treated with viscoelastic constrained layer damping*. Tianjin, China: Tianjin University, 2014.
4. Dong-Xu LI, Liu W and Jiang JP. Passive vibration control of space truss structure with viscoelastic dampers. *Noise Vibrat Control* 2011; 31: 46–50.
5. Jia BX, Gao F and Bian WF. Vibration control of space truss structure with viscoelastic laminated composite damper. *Adv Mater Res* 2014; 971–973: 860–863.
6. Yan-Wu XU, Wang CJ and Song SG. Vibration control and optimization of space deployed truss structure. *Mach Design Manufact* 2014; 04: 24–29.
7. Park YM and Kim KJ. Semi-active vibration control of space truss structures by friction damper for maximization of modal damping ratio. *J Sound Vibrat* 2013; 332: 4817–4828.
8. Yang J, Xiong J, Ma L, et al. Vibration and damping characteristics of hybrid carbon fiber composite pyramidal truss sandwich panels with viscoelastic layers. *Composite Struct* 2013; 106: 570–580.
9. Liu C. *Vibration characteristics and vibration reduction of composite truss*. Harbin, China: Harbin Institute of Technology, 2012.
10. Pei LI, Qinwei MA, Song YP, et al. Deployment dynamics simulation and ground test of a large space hoop truss antenna reflector. *Scientia Sinica* 2017; 47: 104602.
11. Liu MF and Chang TP. Vibration analysis of a magnetoelastic beam with general boundary conditions subjected to axial load and external force. *J Sound Vibrat* 2005; 288: 399–411.
12. Luo J, Xie LC, Zhang Y, et al. Vibration control of large space truss antenna and optimization of actuator position. *Equip Environ Eng* 2016; 13: 112–116.
13. Singh M and Heong SC. Cohesive-shear-lag model for cycling stress-strain behavior of unidirectional ceramic matrix composites. *Int J Damage Mech* 2015; 12: 45–64.
14. Minami S, Yamazaki S and Ishii D. Mathematical expression for stress-strain relationship of steel materials. *J Struct Eng B* 2004; 50: 361–365.
15. Lemerle P. Measurement of the viscoelastic properties of damping materials: adaptation of the wave propagation method to test samples of short length. *J Sound Vibrat* 2002; 250: 181–196.
16. Chao W, Zhenhua L and Gu Y. Design methods of constrained damping specimen used in measurement of viscoelastic damping material's mechanics parameters. *China Mech Eng* 2016; 27: 1208–1214.
17. Rousseau M, Haddad F and Gourinat Y. An apparatus for the characterization of damping properties of nonlinear viscoelastic sheared materials. *Mécanique Industries* 2002; 3: 271–2788.
18. Nagasako N, Jahnátek M, Asahi R, et al. Anomalies in the response of V, Nb, and Ta to tensile and shear loading: Ab initio density functional theory calculations. *Phys Rev B Condense Matter* 2010; 20: 760–762.

19. Sun N, Zhu KJ, Liu B, et al. Application study of viscoelastic damping material for the anti-galloping of overhead transmission lines. *Adv Mater Res* 2014; 884–885: 269–272.

20. Sakallı Ö, Kerpiççi H and Kuddusi L. A study on optimizing the energy consumption of a cold storage cabinet. *Appl Thermal Eng* 2017; 112: 424–430.

21. Sezai T. B-1-192 direction of arrival and magnitude estimation by the prony method with consideration of damping factor. In: *Proceedings of the IEICE general conference*, 1 March 2016. Tokyo, Japan: The Institute of Electronics, Information and Communication Engineers.

22. Vo-Duy T, Ho-Huu V, Dang-Trung H, et al. A two-step approach for damage detection in laminated composite structures using modal strain energy method and an improved differential evolution algorithm. *Composite Struct* 2016; 147: 42–53.

23. Liu P, Zheng H, Cai C, et al. Analysis of disc brake squeal using the complex Eigenvalue method. *Appl Acoustics* 2007; 68: 603–615.

24. Zeinoddini M, Nikoo HM and Estekanchi H. Endurance Wave Analysis (EWA) and its application for assessment of offshore structures under extreme waves. *Appl Ocean Res* 2012; 37: 98–110.

25. Rao MD, Echempati R and Nadella S. Dynamic analysis and damping of composite structures embedded with viscoelastic layers. *Composites Part B Eng* 1997; 28: 547–554.

26. Wang A and Shang L. Modal analysis and model optimization of space science experimental equipment. *Eng Test* 2017; 57: 1–4.

27. Kurata N, Kobori T, Takahashi M, et al. Forced vibration test of a building with semi-active damper system. *Earthquake Eng Struct Dyn* 2015; 29: 629–645.

28. Gao W. Reliability-based optimization of active nonstationary random vibration control. *AIAA J* 2015; 43: 1293–1298.